Journal of Energy Chemistry 35 (2019) 30–36

Contents lists available at ScienceDirect

Journal of Energy Chemistry

journal homepage: www.elsevier.com/locate/jechem

http://www.journals.elsevier.com/journal-of-energy-chemistry/

Ti, Zn co-doped hematite photoanode for solar driven photoelectrochemical water oxidation

Quansong Zhu[b], Chunlin Yu[a], Xingwang Zhang[a,*]

[a] Key Laboratory of Biomass Chemical Engineering of Ministry of Education, College of Chemical and Biological Engineering, Zhejiang University, Hangzhou 310027, Zhejiang, China

[b] College of Environmental and Resource Sciences, Zhejiang University, Hangzhou 310027, Zhejiang, China

ARTICLE INFO

Article history:
Received 4 September 2018
Revised 14 October 2018
Accepted 26 October 2018
Available online 1 November 2018

Keywords:
Photoelectrochemical water oxidation
Hematite
Ti
Zn co-doping
DFT calculation

ABSTRACT

Although there have been many reports of metal doping to ameliorate the drawbacks of hematite as the photoanode for water oxidation, most of them focused on monometallic doping, and only a few of them payed attention to bimetallic doping. What is worse, the synergetic mechanism between two metal dopants was not sufficiently studied, especially the density functional theory (DFT) calculation. In this work, the n-type hematite was synthesized by introducing Ti dopant into hematite through the hydrothermal method, and dipping-sintering treatment was employed to further introduce homogeneously dispersed Zn dopant into that, forming the Ti, Zn co-doped hematite. Under the optimal condition, Ti-doped hematite photoanode reached approximately 2-times enhancement of the photocurrent density compared with the pristine one at 1.23 V vs. RHE, while Ti, Zn co-doped hematite anode obtained another 25% elevation. UV–Vis spectroscopy, Mott–Schottky plots, EIS analysis, photo-oxidation of hole scavenger (H_2O_2), and DFT calculation were employed to understand the role of Ti, Zn dopant. Based on the obtained results, the synergetic mechanism of two dopants was discussed, i.e., the improvement of PEC performance of Ti, Zn co-doped hematite photoanode was possibly attributed to greater carrier density and improved charge separation efficiency at the surface of hematite. This work provides new strategy and understanding of the improvement of PEC performance of hematite by doping engineering.

1. Introduction

Long-term excessive utilization of fossil fuels for energy has aroused a series of environmental problems, among which standing out the global warming [1]. As one of the methods, photoelectrochemical cell device, which has been developed to address this problem by using solar energy more efficiently, can split water to oxygen and hydrogen, thus transferring unstable solar energy to storable chemical energy [1–4]. Numerous semiconductors, including TiO_2, WO_3, $BiVO_4$ and α-Fe_2O_3 [5–9], have been studied as photoanode materials in PEC systems. Recently, several studies have proved that α-Fe_2O_3 [5–8] is a promising photoanode toward water splitting as a result of high stability in alkaline solutions, narrow band gap (1.9–2.2 eV) [5], proper valance band position and earth abundant [6]. However, the particularly low electron mobility (10^{-2} cm^2 V^{-1} s^{-1}) [5], and ultrafast recombination of excited electrons and holes (~10 ps) of hematite [7], have greatly restricted its quantum efficiency and severely reduced its PEC performance.

Many strategies have been developed to solve these two problems, such as surface catalysts loading, incorporation of impurities [5,6,8], and construction of passivation interlayers [10,11]. Incorporation of impurities is a simple and effective method to increase its conductivity and reduce recombination, therefore, various dopants, such as Ti [6], Sn [7], Mn [8], Zr [12], and S [5], have been proven to elevate its PEC performance. Among all these dopants, Ti stands out as it can increase the photocurrent significantly through enhanced electrical conductivity and carrier density [10,13,14]. However, when it comes to the recombination of electrons and holes, the positive effect aroused by Ti doping is comparatively limited [15,16]. Besides, it has been reported that Ti doping may reduce the number of active sites on the surface of hematite, thus cast a negative effect on the PEC performance [17]. The issue how to foster the separation of electrons and holes still lies at the heart position.

Several modifications have been developed to ameliorate it, including the construction of passivation layers [10], catalyst loading [18], and building heterojunction [19,20]. Bimetallic doping is an

* Corresponding author.
E-mail address: xwzhang@zju.edu.cn (X. Zhang).

https://doi.org/10.1016/j.jechem.2018.10.012

important and facile way to elevate the conductivity and reduce recombination simultaneously [21–23]. Jun Wang et al. [21] had synthesized Co, Sn co-doped hematite and found that Sn could increase the conductivity of the hematite, while Co fostered the surface reaction. Ali et al. [22] fabricated In, Sn co-doped hematite by inserting an ITO layer and demonstrated that they can reduce the recombination of electrons and holes. Si, Ti [23] and Sn, Zr [24] co-doped hematite had also been investigated before. Although there have been some reports of bimetallic doping hematite, the synergetic mechanism between two dopants is not studied and discussed sufficiently, especially the density functional theory (DFT) calculation, which needs more efforts to dig into.

Here we adopted Zn doping as the strategy to reduce the recombination, as Zn could foster the separation of electrons and holes at the surface [19,20]. We synthesized efficient Ti, Zn co-doped hematite photoanodes for solar driven water oxidation through a facile two-step method, i.e., the hydrothermal method and followed by dipping-sintering treatment, which homogeneously introduced two dopants into hematite. The previous report of Ti,Zn co-doped hematite [6] payed more attention to the elevated carrier concentration, and the function of Zn dopant, as well as the synergetic mechanism need further study. In this work, combining the enhanced conductivity and carrier density aroused by Ti dopant, with reduced electrons-holes recombination aroused by Zn dopant, a 2.5 times enhancement of the photocurrent density than that of pristine hematite photoanode was achieved, thus providing a new strategy to address the intrinsic problems of hematite photoanodes. The careful characterizations and density functional theory calculation were conducted to reveal the possible mechanism of the enhanced PEC performance, and the coordination between two dopants was discussed.

2. Experimental

2.1. Preparation of hematite nanostructure

A 50 mL Teflon-lined stainless steel autoclave was filled with 20 mL aqueous solution containing 0.15 M $FeCl_3{\cdot}6H_2O$, 0.2 M NaF and 0.5 mL ethanol at pH 1.8 (adjusted by 1 M HCl solution). A piece of FTO glass slide was put into the autoclave and heated at 120 °C for 6 h. A uniform layer of FeOOH film was formed on the FTO substrate. It was then washed with deionized water to remove any residual salt, and subsequently sintered in air at 550 °C for 2 h first, with a ramping rate of 5 °C/min, followed by sintering at 700 °C for another 10 min. After the sintering process, the FeOOH nanostructure was completely converted to α-Fe_2O_3 nanostructure.

Ti-doped hematite was prepared by the same procedure for undoped hematite, except various amounts (0.05–0.30 mL) of $TiCl_4$ ethanol was added into the solution mixture as the Ti precursor. The $TiCl_4$ ethanol was prepared by dissolving 160 µL $TiCl_4$ in liquid form into 8 mL ethanol.

Ti, Zn co-doped hematite was fabricated based on the Ti-doped FeOOH nanostructure, which was prepared through the above process. After the Ti-doped FeOOH film was washed with deionized water and dried in air, it was immersed into $Zn(Ac)_2$ ethanol solution with different $Zn(Ac)_2$ concentrations (15–35 mM) for 1 min, and then taken out, dried in the air, gone through the same sintering procedure as undoped hematite, to obtain hematite with various Zn dopant density.

2.2. Structural characterization

The scanning electron microscopy (SEM) and energy dispersive spectroscopy (EDS) spectra were collected by a SU-70 (HITACHI, Japan) field emission scanning electron microscopy. A field emission transmission electron microscope (Tecnai G2 F20 S-TWIN), which is equipped with energy-dispersive X-ray spectrometer was used to obtain the transmission electron microscopy (TEM) and elements mapping characterization, at the accelerating voltage of 200 kV. X-ray photoelectron spectra (XPS) were collected by Escalab 250Xi (Thermo Fisher Scientific) X-ray photoelectron spectrometer with a Mg K_α X-ray resource, using the C 1*s* peak at 284.8 eV as the internal standard. A UV-3150 UV–Vis spectrophotometer was employed to collect the UV–Vis spectra over the range of 350–700 nm.

2.3. Photoelectrochemical characterization

The photoelectrochemical characterizations of hematite photoanodes were performed in a three-electrode system, with a Bio-Logic VSP potentiostat. The prepared pristine/Ti doped/Ti, Zn co-doped hematite photoanodes served as the working electrode, and a high pure platinum plate with an area of 1 cm × 1 cm was employed as the counter electrode. Hg/HgO was used as the reference electrode. A 500 W Xe short arc lamp solar simulator (Aulight, Beijing, CEL-S500) with an AM 1.5 G filter was employed to give the simulated one sun illumination. Its intensity was calibrated to 100 mW/cm^2 with an AM 1.5 G filter by an irradiatometer (Aulight, Beijing, CEL-VIS 400). All the photoelectrochemical measurements were done in 70 mL of 1 M NaOH electrolyte. The reversible hydrogen electrode (RHE) was used to reference the potentials.

Linear sweep voltammetry was carried out with a scan rate of 10 mV/s. Electrochemical impedance spectroscopy (EIS) was measured on the working electrode at a constant applied potential of 0.1 V vs. RHE under simulated 100 mW/cm^2, and the sweeping the frequency changed from 200 kHz to 60 mHz. Mott–Schottky measurements were performed at a frequency of 100 Hz under dark condition. The previously reported equation was employed to calculate [2]. The photo-oxidation of H_2O_2 was performed by the same procedure as LSV test for water oxidation, except 0.5 M H_2O_2 was added into the 1 M NaOH electrolyte.

3. Results and discussion

We fabricated Ti-doped hematite film on the fluorine-doped tin oxide (FTO) glass firstly through the hydrothermal method, using $TiCl_4$ as the dopant source. Homogeneous Zn-doping was achieved through a simple dipping-sintering post treatment by $Zn(Ac)_2$. The optimal Ti-doped hematite and Ti, Zn co-doped hematite were obtained by varying the concentration of two dopant precursors. The optimal Ti-doped hematite (when adding 0.15 mL $TiCl_4$ ethanol solution into the autoclave) was termed as Ti doped anode in the following discussion, with a Ti dopant concentration of approximately 3% (the atomic ratio of Ti/Fe), while the optimal Ti, Zn co-doped hematite (followed by dipping into 15 mM $Zn(Ac)_2$ ethanol solution) was termed as Ti, Zn co-doped anode, with another Zn dopant concentration of about 1.2% (the atomic ratio of Zn/Fe) given by SEM-EDS.

Fig. 1 shows the scanning electron microscope (SEM) images (top view) of the pristine hematite, Ti doped hematite and Ti, Zn co-doped hematite. The original hematite exhibited a uniform morphology of nanorods (Fig. 1(a)), whereas the morphology of hematite changed significantly (Fig. 1(b)) after the introduction of $TiCl_4$, which showed a porous nanostructure like nanocubes. The similar morphology changes after Ti doping have been reported before [20,25]. Contradictory to the previous report [26] about $Zn(Ac)_2$ treatment, which formed an overlayer of ZnO above hematite, the process of dipping-sintering applied to β-FeOOH did not change the morphology (Fig. 1(c)), indicating that Zn was incorporated into the bulk of Ti doped hematite, rather than deposited on the surface of it.

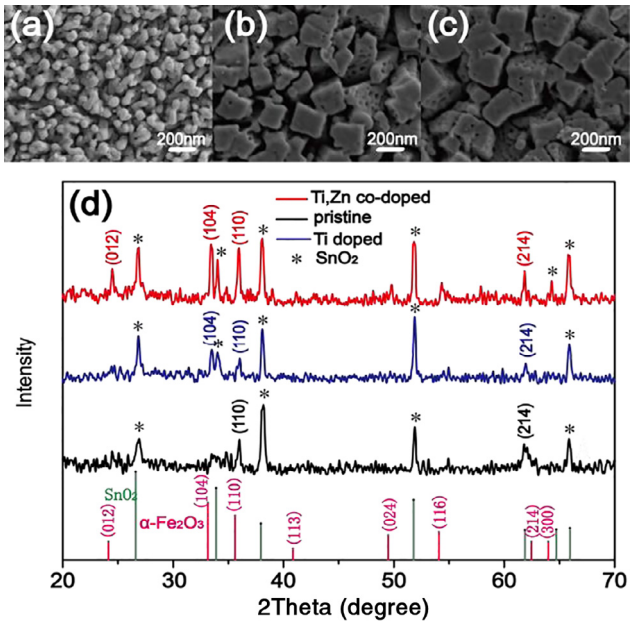

Fig. 1. SEM images of (a) pristine hematite, (b) Ti doped hematite, (c) Ti, Zn co-doped hematite. (d) XRD patterns of pristine hematite, Ti doped hematite, Ti, Zn co-doped hematite. The green and pink lines show the characteristic diffraction peaks of hematite (JCPDS 33-0664) and SnO_2 (JCPDS 41-1445), respectively.

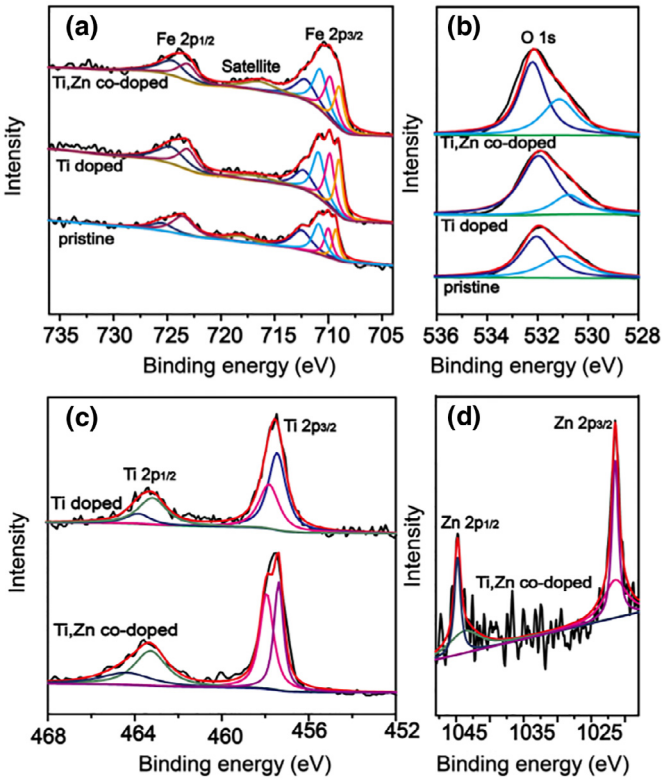

Fig. 2. XPS spectra for pristine hematite, Ti doped hematite and Ti, Zn co-doped hematite: (a) Fe 2*p*, (b) O 1*s*, (c) Ti 2*p*, (d) Zn 2*p*.

The X-ray diffraction (XRD) analysis was applied to characterize the crystal structures of the produced thin films as shown in Fig. 1(d). Generally, the XRD pattern were composed mainly of the characteristic diffraction peaks of the FTO substrate, companied by the characteristic peaks of hematite. Obviously, the number and intensity of characteristic hematite peaks grew with the introduction of Ti-dopant, followed by Zn-dopant, indicating their better crystallinity compared with pristine hematite. Previous studies have pointed out that better crystallinity could reduce the number of defects, thus reducing the recombination of electrons and holes [27–29]. So Ti, Zn dopant might reduce the recombination of charges through enhancing its crystallinity. Other lattice designates of Ti, Zn, as well as their hybrid oxide were not observed, further indicating that Ti, Zn-dopant were uniformly incorporated into the bulk.

The X-ray photoelectron spectroscopy (XPS) analysis was conducted on pristine hematite, Ti doped hematite, and Ti, Zn co-doped hematite to verify the diffusion of Ti and Zn dopants into hematite and determine the chemical states of them. The survey spectrum was shown in Fig. S1, while Fig. 2 was the high resolution spectrum for Fe, O, Ti and Zn. Fig. 2(a) shows the typical Fe $2p_{1/2}$ and Fe $2p_{3/2}$ peaks. The absence of satellite peaks of Fe^{2+} at 730 or 715 eV indicated that Fe^{2+} does not exist at the surface. Fig. 4(c) indicates that Ti dopant was at +4 state, due to its $2p_{1/2}$ peak at 463.7 eV and $2p_{3/2}$ peak at 458.2 eV. The $2p_{1/2}$ peak, and $2p_{3/2}$ peak, respectively at 1044.1 eV and 1020.6 eV, confirmed the existence of Zn on the surface, which was consistent with the previous report [30].

To further examine the crystal structure and distribution of dopants in hematite electrodes, transmission electron microscope (TEM) analysis, as well as EDX elemental mapping, was employed on Ti, Zn co-doped hematite (Fig. 3). Well-resolved lattice fringes with interplanar distance of 2.6 Å were observed (Fig. 3(b)), corresponding to the (104) plane of hematite. Both the two dopant distributed homogeneously in hematite (Fig. 3(c)–(g)), providing the direct evidence for uniform distribution of dopants in hematite by the two-step method.

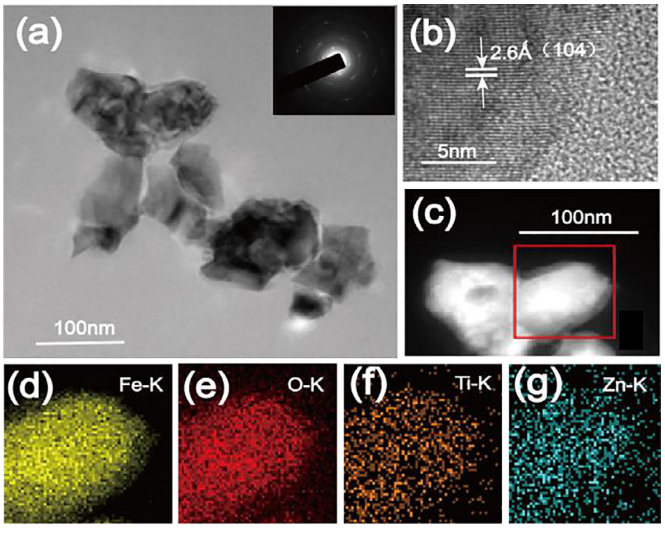

Fig. 3. Ti, Zn co-doped hematite: (a) TEM image, (b) HRTEM image, (c)–(g) EDX elemental mapping of Fe, O, Ti and Zn.

UV–Vis spectra of pristine hematite, Ti doped hematite and Ti, Zn co-doped hematite were shown in Fig. 4(a). It was seen that the pristine hematite exhibited a relatively lower absorption of light with wavelengths of 350–450 nm compared with other two electrodes, while Ti, Zn co-doped hematite shows slightly weaker absorption than Ti doped hematite. The calculated band gaps, based on the Tauc's analysis, turned out to be nearly identical for three samples (Fig. 4(b)), approximately as 2.13 eV, demonstrating that the level of doping was relatively low.

The PEC performance of these three electrodes for water oxidation was investigated in a typical three-electrode system in

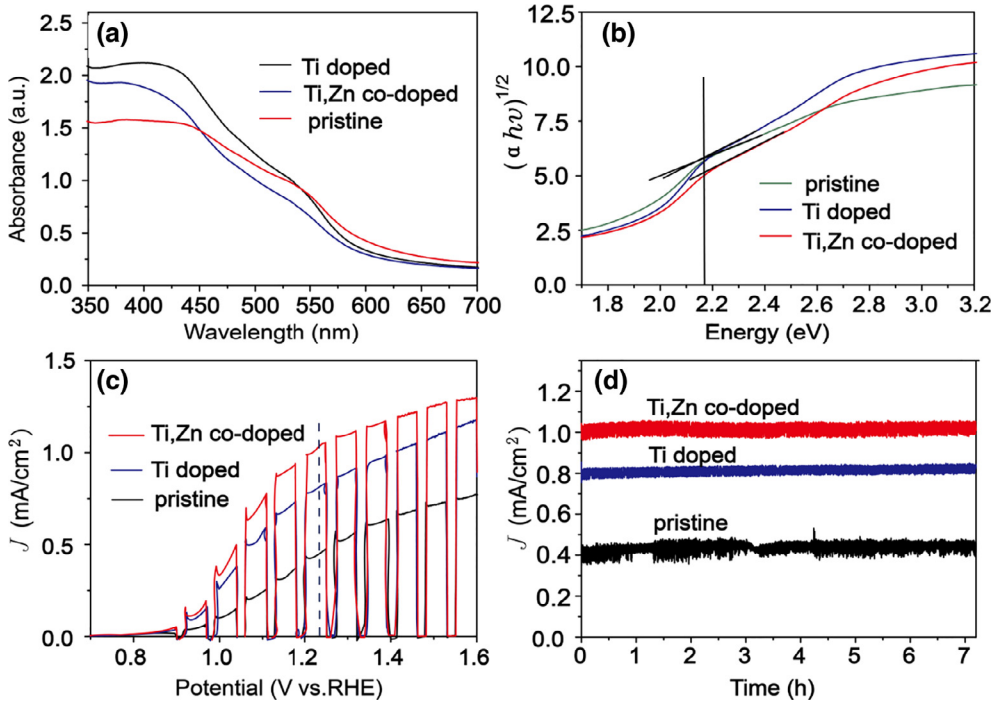

Fig. 4. (a) UV–Vis spectra, (b) Tauc-plots, (c) chopped LSV curves, (d) stable-test curves of pristine photoanode, Ti doped photoanode, and Ti, Zn co-doped photoanode. The LSV test was taken under AM 1.5 G illumination (100 mW cm^{-2}) from the front side.

1 M NaOH. It was found that the introduction of Ti dopant enhanced the current density from 0.43 mA cm^{-2} to 0.80 mA cm^{-2} at the bias of 1.23 V vs. RHE. The maximum photocurrent density was achieved after the introduction of Zn dopant, increasing to 1.02 mA cm^{-2}. Moreover, the stability test showed that no reduction of photocurrent density was observed after 7 h illumination (Fig. 4(d)).

The PEC performance of other Ti, Zn co-doped hematite electrodes with different doping fractions was shown in Fig. S2. The photocurrent densities were elevated as the concentration of Ti dopant increased from 1% to 3%, and further got reduced when reaching 6%. The introduction of Zn dopant into pristine hematite would wipe off its photoelectric response. As abundant studies have pointed out, element Zn is a p-type dopant for hematite which could turn hematite from n-type to p-type, thus enhancing photocathodic current and benefitting hydrogen production [30–32]. So the detrimental effect aroused by Zn dominated the Zn doped hematite, causing it to lose photo response. However, for each group (fractions of Ti dopant were same) of Ti-doped hematite electrodes, a small amount of Zn dopant could facilitate the PEC performance, although a relatively large amount would cast a negative effect on that. Besides, these data showed the tendency that the higher Ti-doping level, the higher Zn-doping level it could hold to elevate PEC performance.

Mott–Schottky (M–S) plots were applied to investigate band structures of these electrodes (Fig. 5(a)). The electrodes were tested in 1 M NaOH without illumination, and the M–S plots were recorded at 100 Hz. The positive slopes of all three electrodes indicated that they all belong to n-type semiconductors, and there were no significant differences between three electrodes about flat band potentials, which were around 0.83 V vs. RHE (Fig. 5(a)). The carrier concentration of the pristine hematite reached 8.16×10^{18} cm^{-3}. Notably, the introduction of Ti dopant achieved a three order elevation of carrier concentrations, reaching 1.26×10^{21} cm^{-3}, similar to the report of Wang et al. [14]. This significant improvement of carrier density might contribute

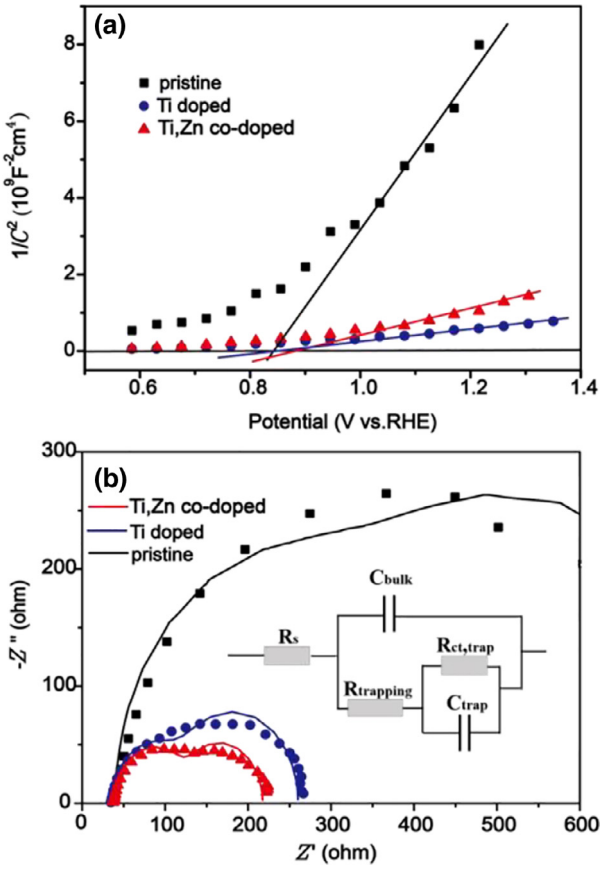

Fig. 5. (a) M–S plots, (b) EIS analysis of pristine hematite, Ti doped hematite, and Ti, Zn co-doped hematite.

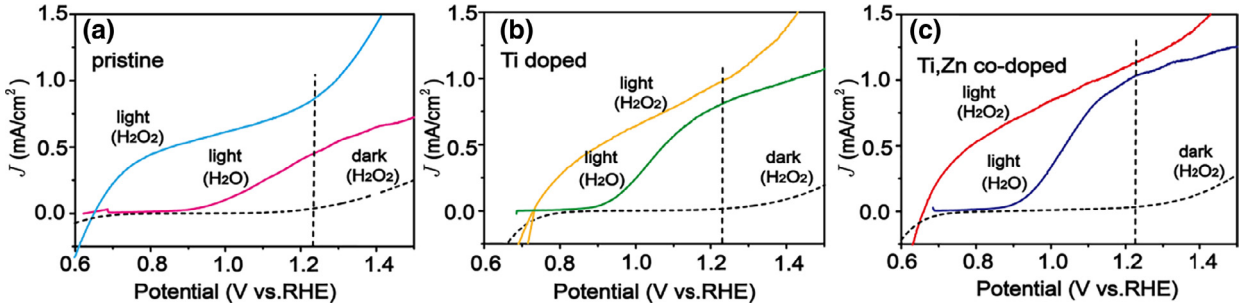

Fig. 6. J–V curves for the photo-oxidation of H_2O_2 and water: (a) pristine photoanode, (b) Ti doped photoanode, (c) Ti, Zn co-doped photoanode. The test was conducted in the electrolyte containing NaOH (1 M) and H_2O_2 (0.5 M) under AM 1.5 G illumination (100 mW cm^{-2}) from the front side.

Table 1. Semiconductor properties of pristine hematite, Ti doped hematite, Ti, Zn co-doped hematite.

	R_s (Ω cm^2)	C_{bulk} (F cm^{-2})	$R_{trapping}$ (Ω cm^2)	C_{trap} (F cm^{-2})	$R_{ct,trap}$ (Ω cm^2)
Pristine hematite	39.6	3.1×10^{-5}	425.2	2.3×10^{-3}	319.8
Ti doped	35.9	1.2×10^{-4}	103.3	1.1×10^{-3}	121.2
Ti, Zn co-doped	38.8	8.2×10^{-5}	95.38	1.5×10^{-3}	83.4

to its high photocurrent [6,14]. It was found that the further introduction of Zn dopant showed a little lower carrier concentration, i.e., 5.61×10^{20} cm^{-3}. Therefore, the improved PEC performance of Ti, Zn co-doped could not be possibly ascribed to the changes of carrier concentrations, nor the flat band potential.

To further understand the role of dopant, electrochemical impedance spectroscopy (EIS) analysis was adopted, as shown in Fig. 5(b). The electric analog we adopted to fit EIS data was given in the inset figure and the corresponding parameters calculated were summarized in Table 1. $R_{trapping}$ represents the resistance for surface state trapping holes and electrons, and $R_{ct,trap}$ described the resistance of charge transfer of holes to reducers in solution. The capacitance of space charge, as well as connection of Helmholtz capacitance, were integrated into C_{bulk}. Besides, C_{trap} denoted the trap-state capacitance, and R_S was the series resistance of the cell [20]. Although no significant differences could be observed of R_S, C_{bulk}, and C_{trap}, the reduction of $R_{trapping}$ and $R_{ct,trap}$ was obtained by incorporating dopant into pristine hematite. This indicated that the surface recombination of holes and electrons was reduced by Ti dopant, further by Zn dopant, and the charge transfer of holes to reducers in solution was fostered. The ameliorated surface reaction may explain the improved PEC performance of Ti doped hematite, and Ti, Zn co-doped hematite [6,33].

We then investigated the photo-oxidation of a hole scavenger (H_2O_2), to further prove the conjecture that the elevated charge separation efficiency contributed to the enhanced water oxidation reactivity. As the surface charge separation of H_2O_2 oxidation is sufficient due to its fast kinetics [34], comparisons of its photocurrents with water oxidation photocurrents gave the extent of surface charge separation efficiency [35,36]. The gap between two LSV curves of oxidation of water and H_2O_2 (0.42 mA/cm^2) was greatly reduced (0.23 mA/cm^2) after the introduction of Ti dopant (Fig. 6(a) and (b)), while the additional Zn dopant continued to reduce the gap to 0.11 mA/cm^2 (Fig. 6(c)). More quantitively, the surface charge separation efficiency (τ_{surf}) could be calculated with the following equation [34]:

$$\tau_{surf} = J^{H_2O}/J^{H_2O_2}$$

The calculated τ_{surf} for pristine hematite, Ti doped hematite, Ti, Zn co-doped hematite was 50.6%, 77.7%, and 90.3% respectively, indicating that the reduced electron-hole recombination and improved charge separation efficiency at the surface could be achieved by Ti doping and Ti,Zn co-doping. Besides, the bulk separation efficiency could be obtained by calculating $J^{H_2O_2}/J_{abs}$, while J_{abs} is the photocurrent density resulting from an absorbed photo conversion efficiency (APCE) of 100%, which can be calculated by integrating the number of photons above the bandgap energy through absorption spectrum (Fig. 4(a)) [37–39]. As shown in Fig. 4(a), while Ti doped hematite absorbed more photons than Ti,Zn co-doped hematite, $J^{H_2O_2}$ for the latter is greater than that for the former (Fig. 6(b) and (c)), which can lead to the conclusion that the charge separation efficiency in the bulk is further improved through the introduction of Zn dopant. What is more, Fig. S5 shows the photocurrent density versus time under chopped light at 1.23 V vs. RHE, the smaller spikes of Ti, Zn co-doped hematite compared with Ti doped hematite, also suggesting enhanced overall charge separation efficiency [2,38,39].

The density functional theory (DFT) calculation was also applied to understand the effects aroused by dopant. It was performed by using the CP2K package [40]. PBE function [41] with Grimme D3 correction [42] was used to describe the system (see SI for calculation details). The calculated band gap of α-Fe_2O_3 was 2.31 eV (Fig. 7(a)). The Fe 3*d* state mainly contributed to the CBM, while the VBM was primarily composed of Fe 3*d* and O 2*p* orbits. After 3% Fe atoms were substituted by Ti atoms (Fig. 7(b)), the valence band was significantly interrupted by Ti doping. Besides, the valence band edge shifted toward the conduction band for around 0.48 eV, while the conduction band moved negatively for about 0.12 eV (the calculated band gap edge positions were listed in Table S1), so the band gap shrank by about 0.6 eV. Such an obvious shrink of band gap indicated the extra electrons provided by Ti [16], consistent with the outcome of M–S plots (Fig. 5(a)). The electron provided by Ti 3*d* orbit can flow to nearby Fe 3*d* orbit [16], so the increased donor density and enhanced conductivity should be one of the reasons for better PEC performance of Ti doped than α-Fe_2O_3. In contrast, the incorporation of Zn had little impact on the band structure of α-Fe_2O_3 (Fig. S4). Significant changes could hardly be found when comparing the density of states (DOS) plots of α-Fe_2O_3 and Zn doped hematite. When it comes to incorporating Zn into Ti doped (Fig. 7(c)), the conduction band edge shifted positively for about 0.12 eV, while the valence band edge position remained the same. It seemed that Zn dopant brought little impact to the band structure of Ti doped hematite, so other reasons, except the band structure, might also explain the enhancement aroused by Zn dopant.

Comprehensively speaking, the positive effect of Zn dopant lies in fostering charge separation in the bulk and at the surface, while it may bring detrimental influence to water oxidation process considering its p-type nature for hematite, which has been discussed above. In contrast, Ti dopant is widely believed to be a n-type dopant [16,17,43], and it can enhance the conductivity of hematite significantly, but its positive effect on charge separation is limited [15,16]. Co-doping both elements can make n-type Ti dopant off-

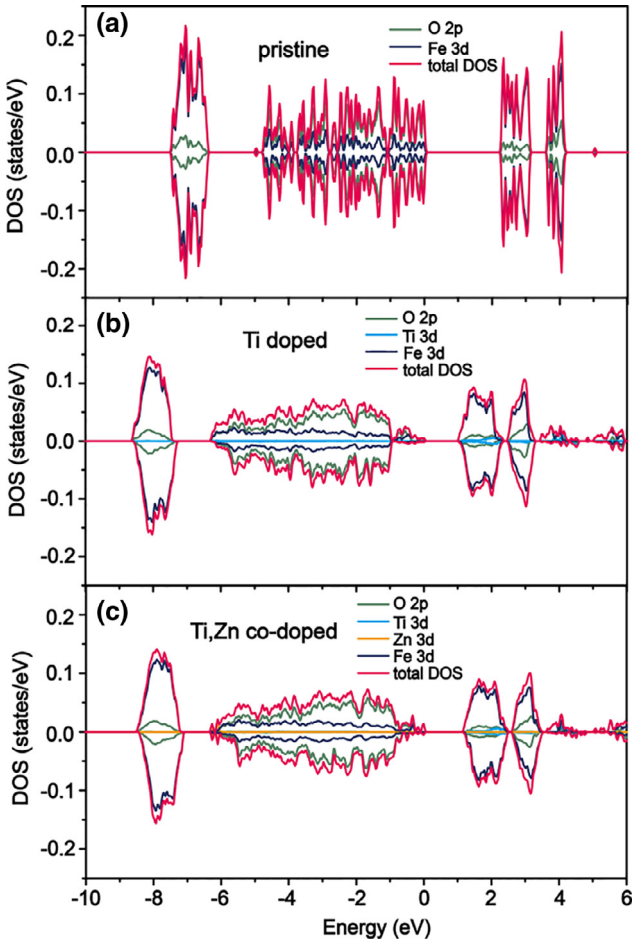

Fig. 7. DOS of (a) pristine hematite, (b) Ti doped hematite, (c) Ti, Zn co-doped hematite.

set negative effect aroused by p-type Zn dopant, while utilizing Zn's positive effect on charge separation to compensate Ti's limited influence on that. Two dopants work together to achieve an overall better performance by balancing their respective pros and cons, and this is where the synergetic mechanism between two dopants lies. The detrimental effect of Zn dopant may overweigh its positive effect when the concentration of Ti dopant is low, or the concentration of Zn goes too high, as shown in Fig. S2. Therefore, the good quantity control of dopant concentration should be attached with great importance in order to coordinate two dopants well enough for achieving higher photocurrent density.

Although several reports have shown the potential benefits of n,p co-doping based on DFT calculation [16,44,45], experimental work for verification is rare. This work experimentally proved the benefits of n,p co-doping, and pointed out the coordination mechanism between n-type dopant and p-type dopant. Rational design to construct bimetallic or multi-metallic doped hematite should consider respective pros and cons of different dopants and potential synergetic mechanism between them in order to strike a balance and achieve the best overall performance.

4. Conclusions

In summary, homogeneous Ti, Zn co-doping could be an effective way to enhance the PEC performance of hematite. While the enhancement aroused by Ti doping could be attributed to increased carrier density (a three order elevation) and higher electrons and holes separation efficiency, the further elevation aroused by Zn dopant should be mainly explained by reduced electrons-holes recombination in the bulk and at the surface. As the introduction of excessive Zn dopant might turn weak n-type hematite to p-type, it is important to control the concentration of Zn dopant for the optimal PEC performance, and enhancing the n-type property of hematite through Ti doping could be a useful method. This work provides experimental verification for the n,p co-doping which has been theoretically studied, pointing out the coordination effects between two kinds of dopants, as well as the importance of controlling their respective quantities to balance their pros and cons.

Notes

The authors declare no competing financial interest.

Acknowledgments

This research was supported by Major Science and Technology Project of Water Pollution Control and Management (No. 2017ZX07101003) and Zhejiang Provincial Natural Science Foundation of China under Grant no. LR17B060003. The author Quansong Zhu wants to give special thanks to BirdyC for her support and care over the past year. You are the luck I want to keep most. The work was also financially supported by the Natural Science Foundation of China (Project Nos. 21436007, 21522606, 21476201, 21676246, U1462201, and 21776248).

Supplementary materials

Supplementary material associated with this article can be found, in the online version, at doi:10.1016/j.jechem.2018.10.012.

References

[1] S. Chu, W. Li, Y. Yan, T. Hamann, I. Shih, D. Wang, Z. Mi, Nano Futur. 1 (2017) 022001.
[2] W. Liu, H. Liu, L. Dang, H. Zhang, X. Wu, B. Yang, Z. Li, X. Zhang, L. Lei, S. Jin, Adv. Funct. Mater. 27 (2017) 1603904.
[3] X. Gao, H. Zhang, Q. Li, X. Yu, Z. Hong, X. Zhang, C. Liang, Z. Lin, Angew. Chem. 128 (2016) 6398–6402.
[4] H. Zhang, B. Yang, X. Wu, Z. Li, L. Lei, X. Zhang, ACS Appl. Mater. Interfaces 7 (2015) 1772–1779.
[5] R. Zhang, Y. Fang, T. Chen, F. Qu, Z. Liu, G. Du, A.M. Asiri, T. Gao, X. Sun, ACS Sustain. Chem. Eng. 5 (2017) 7502–7506.
[6] N. Mirbagheri, D. Wang, C. Peng, J. Wang, Q. Huang, C. Fan, E.E. Ferapontova, ACS Catal. 4 (2014) 2006–2015.
[7] Y. Ling, G. Wang, D.A. Wheeler, J.Z. Zhang, Y. Li, Nano Lett. 11 (2011) 2119–2125.
[8] Gurudayal, S.Y. Chiam, M.H. Kumar, P.S. Bassi, H.L. Seng, J. Barber, L.H. Wong, ACS Appl. Mater. Interfaces 6 (2014) 5852–5859.
[9] P. Zhang, T. Wang, J. Gong, Chem 4 (2018) 223–245.
[10] Z. Luo, T. Wang, J. Zhang, C. Li, H. Li, J. Gong, Angew. Chem. Int. Ed. 56 (2017) 12878–12882.
[11] S. Shen, S.A. Lindley, X. Chen, J.Z. Zhang, Energy Environ. Sci. 9 (2016) 2744–2775.
[12] S. Shen, P. Guo, D.A. Wheeler, J. Jiang, S.A. Lindley, C.X. Kronawitter, J.Z. Zhang, L. Guo, S.S. Mao, Nanoscale 5 (2013) 9867.
[13] R. Franking, L. Li, M.A. Lukowski, F. Meng, Y. Tan, R.J. Hamers, S. Jin, Energy Environ. Sci. 6 (2013) 500–512.
[14] G. Wang, Y. Ling, D.A. Wheeler, K.E.N. George, K. Horsley, C. Heske, J.Z. Zhang, Y. Li, Nano Lett. 11 (2011) 3503–3509.
[15] J. Velev, A. Bandyopadhyay, W.H. Butler, S. Sarker, Phys. Rev. B (2005) 71.
[16] H. Pan, X. Meng, D. Liu, S. Li, G. Qin, Phys. Chem. Chem. Phys. 17 (2015) 22179–22186.
[17] C. Miao, T. Shi, G. Xu, S. Ji, C. Ye, ACS Appl. Mater. Interfaces 5 (2013) 1310–1316.
[18] K. Dang, T. Wang, C. Li, J. Zhang, S. Liu, J. Gong, Engineering 3 (2017) 285–289.
[19] K.J. McDonald, K.-S. Choi, Chem. Mater. 23 (2011) 4863–4869.
[20] C. Miao, S. Ji, G. Xu, G. Liu, L. Zhang, C. Ye, ACS Appl. Mater. Interfaces 4 (2012) 4428–4433.
[21] J. Wang, C. Du, Q. Peng, J. Yang, Y. Wen, B. Shan, R. Chen, Int. J. Hydrogen Energy 42 (2017) 29140–29149.
[22] A. Kaouk, T.-P. Ruoko, M. Pyeon, Y. Gönüllü, K. Kaunisto, H. Lemmetyinen, S. Mathur, J. Phys. Chem. C 120 (2016) 28345–28353.
[23] M. Zhang, W. Luo, Z. Li, T. Yu, Z. Zou, Appl. Phys. Lett. 97 (2010) 042105.

[24] A.G. Tamirat, W.-N. Su, A.A. Dubale, H.-M. Chen, B.-J. Hwang, J. Mater. Chem. A 3 (2015) 5949–5961.
[25] J. Deng, J. Zhong, A. Pu, D. Zhang, M. Li, X. Sun, S.-T. Lee, J. Appl. Phys. 112 (2012) 084312.
[26] L. Xi, P.S. Bassi, S.Y. Chiam, W.F. Mak, P.D. Tran, J. Barber, J.S. Chye Loo, L.H. Wong, Nanoscale 4 (2012) 4430.
[27] Q. Zhang, Appl. Catal. B: Environ. 26 (2000) 207–215.
[28] F. Amano, A. Yamakata, K. Nogami, M. Osawa, B. Ohtani, J. Am. Chem. Soc. 130 (2008) 17650–17651.
[29] L. Yang, G. Li, W. Hu, M. Zhao, L. Sun, J. Zheng, T. Yan, L. Li, Eur. J. Inorg. Chem. 2011 (2011) 2211–2220.
[30] X. Qi, G. She, M. Wang, L. Mu, W. Shi, Chem. Commun. 49 (2013) 5742.
[31] W.B. Ingler, S.U.M. Khan, Electrochem. Solid-State Lett. 9 (2006) G144.
[32] Z. Fan, X. Wen, S. Yang, J.G. Lu, Appl. Phys. Lett. 87 (2005) 013113.
[33] C. Zheng, Z. Zhu, S. Wang, Y. Hou, Appl. Surf. Sci. 359 (2015) 805–811.
[34] J.Y. Kim, D.H. Youn, K. Kang, J.S. Lee, Angew. Chem. Int. Ed. 55 (2016) 10854–10858.
[35] J.Y. Kim, D.H. Youn, J.H. Kim, H.G. Kim, J.S. Lee, ACS Appl. Mater. Interfaces 7 (2015) 14123–14129.
[36] H. Dotan, K. Sivula, M. Grätzel, A. Rothschild, S.C. Warren, Energy Environ. Sci. 4 (2011) 958–964.
[37] T.W. Kim, K.-S. Choi, Science 343 (2014) 990–994.
[38] D.K. Zhong, S. Choi, D.R. Gamelin, J. Am. Chem. Soc. 133 (2011) 18370–18377.
[39] E.S. Kim, H.J. Kang, G. Magesh, J.Y. Kim, J.-W. Jang, J.S. Lee, ACS Appl. Mater. Interfaces 6 (2014) 17762–17769.
[40] J. Hutter, M. Iannuzzi, F. Schiffmann, J. VandeVondele, Wiley Interdiscip. Rev.: Comput. Mol. Sci. 4 (2014) 15–25.
[41] J.P. Perdew, K. Burke, M. Ernzerhof, Phys. Rev. Lett. 77 (1996) 3865–3868.
[42] S. Grimme, J. Comput. Chem. 27 (2006) 1787–1799.
[43] J. Deng, J. Zhong, A. Pu, D. Zhang, M. Li, X. Sun, S.-T. Lee, J. Appl. Phys. 112 (2012) 084312.
[44] X.Y. Meng, G.W. Qin, S. Li, X.H. Wen, Y.P. Ren, W.L. Pei, L. Zuo, Appl. Phys. Lett. 98 (2011) 112104.
[45] D. Zhang, M. Yang, Phys. Chem. Chem. Phys. 15 (2013) 18523.